

Data Reduction Techniques for the Analysis and Interpretation of Dynamic FDG-PET Oncological Studies

George Kontaxakis, *Member, IEEE*, Trias Thireou, Sotiris Pavlopoulos, *Member, IEEE*, and Andres Santos, *Senior Member, IEEE*

Abstract— Dynamic positron emission tomography studies produce a large amount of image data, from which clinically useful parametric information can be extracted with the use of tracer kinetic methods. In order to facilitate the initial interpretation and visual analysis of these large image sequences, data reduction methods can be applied which at the same time maintain important information and allow basic feature characterization. We show here that the application of principal component analysis can provide high-contrast parametric image sets of lesser dimension than the original ones separating structures with different kinetic characteristics. This method has been shown to be an alternative quantification method, independent of any kinetic model and particularly useful when the retrieval of the arterial input function is complicated. Furthermore, novel similarity mapping techniques are proposed, which can summarize in a single image the temporary properties of the whole image sequence according to a reference region. Based on the newly introduced cubed sum coefficient similarity measure, we show that structures with similar time activity curves similar to the tumor's ones can be identified, thus facilitating the detection of lesions not easily discriminated with the conventional method using standardized uptake values.

I. INTRODUCTION

IN oncology, the visual inspection of the PET images is the practice routinely used for tumor diagnosis, detection of metastases and evaluation of treatment. However, quantitative measures based on the normalization of tracer concentrations for the injected activity and body weight (standardized uptake values, SUV) are becoming common in the clinical praxis in oncological PET studies [1].

SUV-based evaluation requires a well-calibrated PET platform in order to produce quantitatively accurate results. It also reflects the late stage in the process of glucose uptake by tissues ignoring the kinetics of this predominantly dynamic

process, which might be able to provide valuable information on the molecular events that characterize tumor development and associated vasculature, as well as its specific resistance to treatment. In fact, the use of SUV as a method of classification of tissue areas as benign or malign is still under discussion among nuclear medicine physicians and oncologists [2],[3].

Dynamic ^{18}F -FDG PET studies (temporal sequences of images at the same bed position) offer differential diagnostic information and therefore represent an accurate approach to quantify ^{18}F -FDG kinetics. Such studies are been increasingly used in oncological PET studies for diagnosis, therapy management and evaluation [4]. The analysis of dynamic PET sequences, however, often requires complex analysis using compartmental or non-compartmental models, where many difficulties must be overcome, such as the determination of the input function of the concentration of the radioactive tracer in plasma, the intrinsic inaccuracies at the time of selecting the appropriate compartmental model, or time-consuming computations involving a large amount of image data to be processed.

In this work we investigate the use of principal component analysis (PCA) and similarity mapping (SM) techniques in order to reduce the initial amount of image data to a smaller, comprehensive and easily managed set of parametric images. Such methods have the advantage that can produce results in very short time, as they have little computational complexity, and can provide an accurate tool for the support of both the visual inspection and the posterior detailed kinetic analysis of the dynamic series via compartmental or non-compartmental models [5]. Furthermore, the application of independent component analysis (ICA) is briefly discussed, as it has been recently shown to produce promising results in the analysis of task-related functional magnetic resonance imaging (fMRI) techniques [6], as well as in the extraction of the input function in dynamic myocardial PET studies [7]. ICA is a statistical technique that can be used as a method for blind source separation. The observed data are assumed to be unknown linear mixtures of unobserved independent source signals, which can be recovered with no prior information using ICA.

Manuscript received November 1, 2004. This work was supported in part by the "Ramón y Cajal" Program of the Spanish Ministry of Education and Science, the Thematic Network "IM3" of the Spanish Ministry of Health (*Fondos de Investigación Sanitaria, FIS*).

G. Kontaxakis and A. Santos are with the Technical University of Madrid (ETSI Telecomunicación, Departamento de Ingeniería Electrónica, ES-28040 Madrid, tel: +34-91-3367366, ext. 582, e-mail: {gkont, andres}@die.upm.es).

T. Thireou and S. Pavlopoulos are with the National Technical University of Athens (School of Electrical and Computer Engineering, Biomedical Engineering Laboratory, GR-15773 Athens, telephone: +30-210-7723926, e-mail: spav@biomed.ntua.gr, thireou@central.ntua.gr).

II. METHODS

PCA explains the variance-covariance of a set of variables through a few linear combinations of these in order to achieve data reduction and facilitate their interpretation [8]. Although N components are required to reproduce the total system variability, often much of this variability can be accounted for by a small number p of the principal components. These components can then replace the initial N variables, and the original data set, consisting of k measurements on N variables, is reduced to a data set consisting of k measurements on p principal components.

Let $\mathbf{F} = (\mathbf{F}_1, \mathbf{F}_2, \dots, \mathbf{F}_N)$ have covariance matrix: \mathbf{C} with eigenvalue – eigenvector pairs $(\lambda_1, \mathbf{e}_1), (\lambda_2, \mathbf{e}_2), \dots, (\lambda_N, \mathbf{e}_N)$, where $\lambda_1 \geq \lambda_2 \geq \dots \geq \lambda_N \geq 0$. The i^{th} principal component is given by:

$$\mathbf{P}_i = \mathbf{e}_i^T \mathbf{F}_i = e_{i1} \mathbf{F}_{i1} + e_{i2} \mathbf{F}_{i2} + \dots + e_{iN} \mathbf{F}_{iN}, \quad i = 1, 2, \dots, N \quad (1)$$

with $\text{Var}(\mathbf{P}_i) = \mathbf{e}_i^T \mathbf{C} \mathbf{e}_i = \lambda_i$ & $\text{Cov}(\mathbf{P}_i, \mathbf{P}_m) = \mathbf{e}_i^T \mathbf{C} \mathbf{e}_m = 0$ if $i \neq m$

The total population variance is given by:

$$\sum_{i=1}^N \text{Var}(\mathbf{F}_i) = \sum_{i=1}^N \text{Var}(\mathbf{P}_i) = \sum_{i=1}^N \lambda_i \quad (2)$$

Consequently, the proportion of total variance described by the i^{th} principal component is:

$$tv_i = \frac{\lambda_i}{\sum_{m=1}^N \lambda_m}, \quad m = 1, 2, \dots, N \quad (3)$$

Typically the largest part of the total variance can be attributed to the first few principal components, which can be considered as containing the same information (excluding the contribution of noise which can be attributed to the rest of them) as the original data set. For dynamic PET images, these few principal components constitute a reduced set of principal component images (PCI) that can be considered as representing a “summary” of the kinetic information that is contained in original study frames and can therefore be used to extract basic information for an initial evaluation of the dynamic study.

As mentioned before, the main goal of the initial evaluating step for large dynamic oncological PET studies is the accuracy in localizing and staging primary tumors and metastases. Similarity mapping methods create a temporal match of the intensity values of the pixels in the image sequence with the ones of a selected reference region of interest (rROI).

The similarity measures described in the literature [9],[10] applied on dynamic MRI studies are based on the calculation of the correlation (COR) and normalized correlation ($NCOR$) coefficients. We introduce here the following additional measures which are more appropriate for the low contrast PET

image sets: sum of squares (SSQ), squared sum (SQS), sum of cubes (SC) and cubed sum (CS) coefficients:

$$COR_{ij} = \frac{\sum_{n=1}^N V_{ijn} R_n}{\sqrt{\sum_{n=1}^N V_{ijn}^2 \sum_{n=1}^N R_n^2}} \quad (4) \quad NCOR_y = \frac{\sum_{n=1}^N (V_{ijn} - \mu_{vij})(R_n - \mu_R)}{\sqrt{\sum_{n=1}^N (V_{ijn} - \mu_{vij})^2 \sum_{n=1}^N (R_n - \mu_R)^2}} \quad (5)$$

$$SSQ_y = \frac{\sum_{n=1}^N (V_{ijn} - \mu_{vij})^2 (R_n - \mu_R)^2}{\mu_R \sqrt{\sum_{n=1}^N (V_{ijn} - \mu_{vij})^2 \sum_{n=1}^N (R_n - \mu_R)^2}} \quad (6)$$

$$SC_y = \frac{\sum_{n=1}^N (V_{ijn} - \mu_{vij})^3 (R_n - \mu_R)^3}{\mu_R^2 \sqrt{\sum_{n=1}^N (V_{ijn} - \mu_{vij})^2 \sum_{n=1}^N (R_n - \mu_R)^2}} \quad (7)$$

$$SQS_y = \frac{(\sum_{n=1}^N (V_{ijn} - \mu_{vij})(R_n - \mu_R))^2}{\mu_R \sqrt{\sum_{n=1}^N (V_{ijn} - \mu_{vij})^2 \sum_{n=1}^N (R_n - \mu_R)^2}} \quad (8)$$

$$CS_y = \frac{(\sum_{n=1}^N (V_{ijn} - \mu_{vij})(R_n - \mu_R))^3}{\mu_R^2 \sqrt{\sum_{n=1}^N (V_{ijn} - \mu_{vij})^2 \sum_{n=1}^N (R_n - \mu_R)^2}} \quad (9)$$

where N is the frame number in the study, V_{ijn} is the value of pixel (i,j) in frame n , R_n is the value of the time activity curve (TAC) in the rROI, μ_R is the mean value of the TAC of the rROI and μ_{vij} is the mean value of the TAC of pixel (i,j) .

The SM analysis has been based as a first step on synthetic data from a digital phantom shown in Figure 3. This has been created by simulating a single-slice image series from a clinical ^{18}F -FDG PET study of a colorectal tumor recurrence, including the noise characteristics of the measured data.

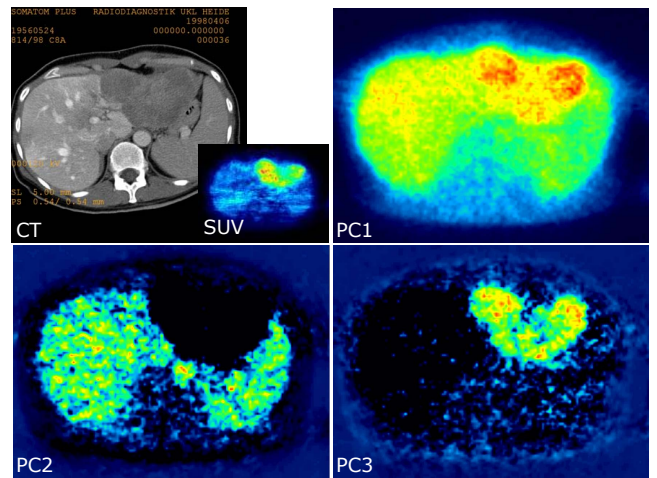


Figure 1: An example of the application of PCA to a dynamic FDG PET study (15 frames, 21 slices/frame, 256x256 image matrix), showing a large lesion on the upper left liver lobe.

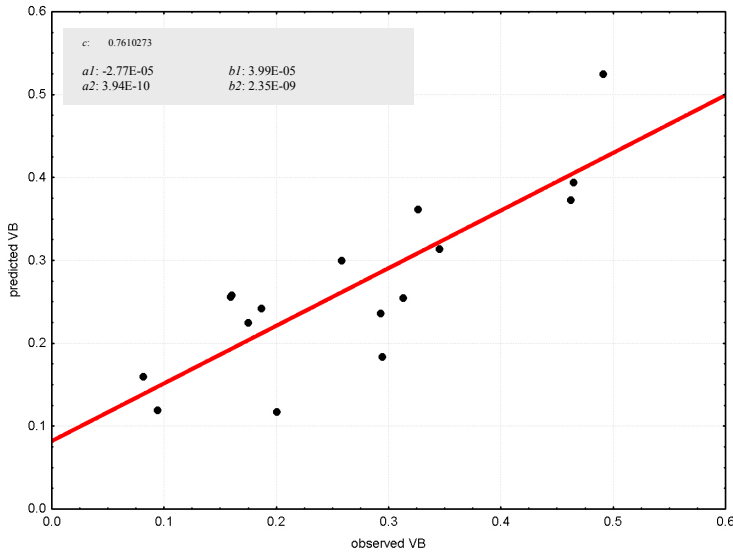


Figure 2: Tumor vascular fraction VB can be estimated from PC11 and PC12. The correlation coefficient of the polynomial regression equals 0.834.

III. RESULTS

A. Application of PCA

The application of PCA to a dynamic PET image sequence (15 frames, 21 slices/frame, 256x256 image matrix), resulted in 15 principal component images (PCI), of which the first one (PC1) resembled to a summed SUV image of all 15 original image frames, where all structures (lesion, vasculature and other high-activity structures) were visible. The second PCI (PC2) showed only the vascular components leaving the area covered by the lesion black, whereas the third one (PC3) contained a bright area corresponding to the lesion. Figure 1 summarizes these results and shows for reference the corresponding CT slice image, as well as the SUV image that corresponds to the late emission part of the dynamic study (summation of the last 4 frames). The rest of the resulting images contained mainly noise.

The results obtained for this case and the initial conclusions drawn have been verified by applying the same analysis to the data obtained from 17 colorectal tumor recurrence clinical studies (23 frames, 32 slices/frame, 128x128 pixels/slice). Only for the PC3 the lesions were clearly visible in 14 of the cases, as in 3 cases their size due to partial volume effects and possibly to the physiologic activity in the surrounding tissues did not allow the direct correlation of PC3 to the tumor. The average proportion of the total variance described by these first 3 principal components, in all 17 studies according to (3) were:

$$tv_1 = 78.3 \pm 2.6, tv_2 = 3.7 \pm 1.0, tv_3 = 1.8 \pm 0.2$$

PCA therefore is able to separate different structures of interest in large dynamic sequences in different PCIs for FDG PET oncological studies.

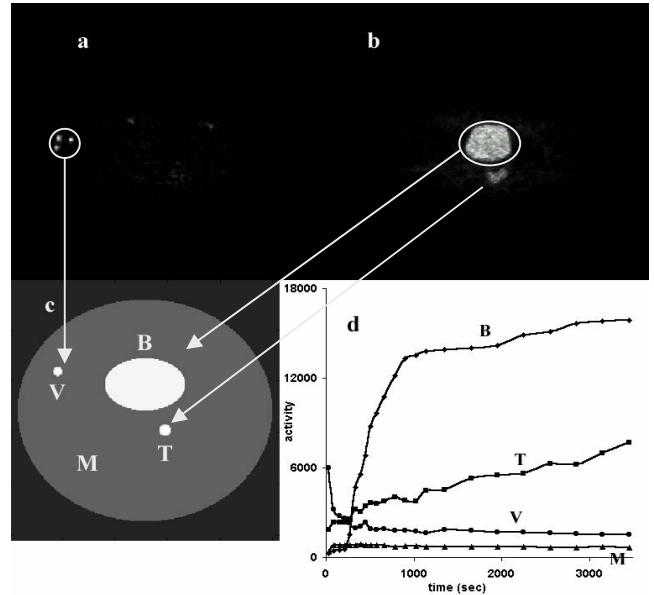


Figure 3: Two frames (a)-(b) of a real dynamic PET study used for the formation of a simulated dynamic PET phantom image series (c). The TACs (d) from the study were used as basis for the definition of the corresponding TAC functions of the phantom. The phantom consists of a big ellipse (M) corresponding to normal tissue mass and three smaller ellipses corresponding to the bladder (B), tumor (T) and a vessel (V).

This approach facilitates the visual analysis of the sequence on the one hand and, although for the application of PCA no region of interest (ROI) is necessary to be drawn, it provides a tool for a more accurate selection of the ROIs on lesions and/or vessels in order to proceed to further parametric analysis of the dynamic sequences.

For the kinetic analysis based on the 2-compartment model, the input function is obtained by continuously extracting blood samples during acquisition. The vascular fraction (VB) must be taken into account for the calculation of the transport constant K1 and the rate constants k2, k3 and k4 for such a kinetic model. We have here investigated the possibility to retrieve the input function from the PCI obtained.

In the resulting PCIs, volumes of interest (VOIs) were placed over the lesions and the surrounding normal tissue in the first two PCI, and the mean counts for each of them were calculated. Polynomial regression up to the second order was used to establish a quantitative relationship between the predictor variables (X_i , mean counts) and the response (VB):

$$VB = c + \sum_{i=1}^2 a_i X_i + \sum_{i=1}^2 b_i X_i^2 \quad (10)$$

The unknown coefficients were computed using a least squares fit, which minimized the sum of the squares of the deviations of the data from the model. Figure 2 shows the polynomial regression line coefficients based on (10) computed for the tumor fractional blood volume estimation. The correlation coefficient is 0.834.

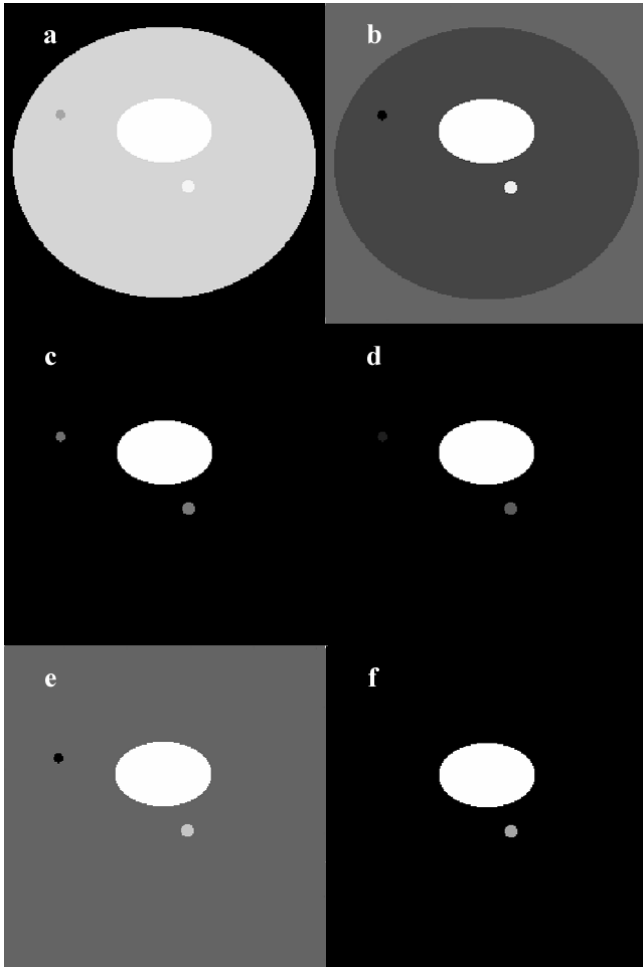


Figure 4: Similarity maps of the simulated dynamic PET study shown in Figure 3, calculated using a reference ROI placed over the bladder and the similarity measures (a) COR, (b) NCOR, (c) SSQ, (d) SQS, (e) SC and (f) CS (f).

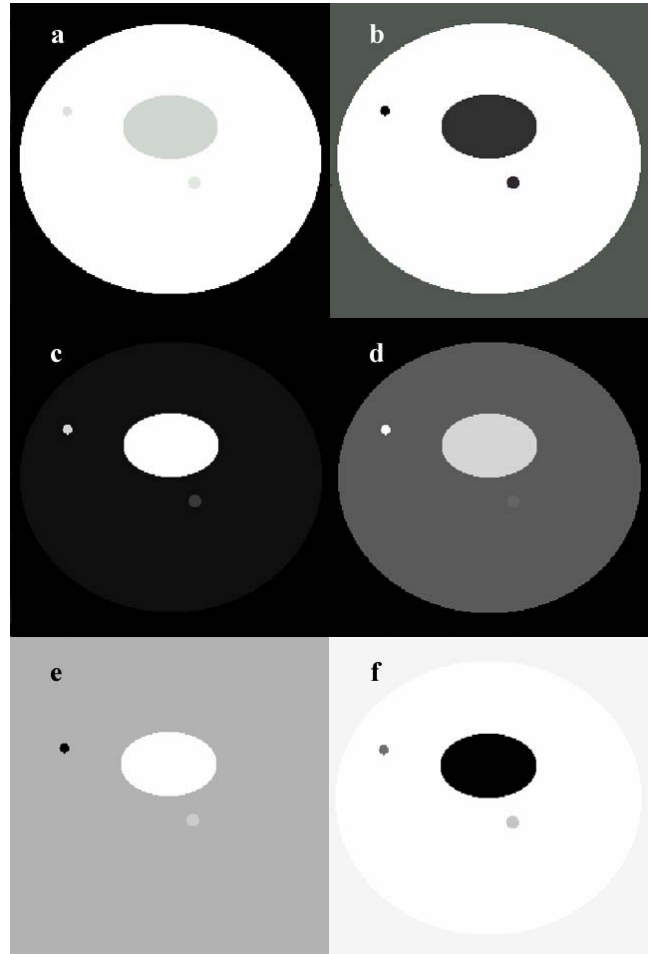


Figure 5: Similarity maps of the simulated dynamic PET study shown in Figure 3, calculated using a reference ROI placed over normal tissue mass and the SM measures (a) COR, (b) NCOR, (c) SSQ, (d) SQS, (e) SC and (f) CS (f).

B. Application of SM

Figure 4 shows the results from the application of the similarity coefficients by placing a ROI over the bladder (ROI_b) of the simulated phantom image series. Figure 5 shows the results after placing the reference ROI over normal tissue mass (ROI_m). The contrast in the resulting images is measured as $CR = (T-M)/M$ (where T and M are the mean activity distributions in ROIs placed over the tumor and normal tissue masses areas respectively).

In the ROI_b case, the tumor can be distinguished in all SM images with different levels of contrast and clarity. The SUV for the lesion was 34 and the CS metric resulted to a contrast value of 54, whereas the COR-image contrast was 0.15 (showing the lesions at similar contrast level with normal tissue) and the NCOR-image reached a contrast level of 2.46. In some of the maps, the vessel can be also distinguished with negative values (shown in black) or positive values (as is the case of the SSQ-image). For the ROI_m case in most of the maps the lesion is visible but has similar (low) contrast levels with the reference muscle tissues in almost all SM images.

When the same approach has been applied to the set of 17 clinical dynamic studies of colorectal lesions mentioned before, the SM based on the correlation coefficient and the normalized correlation coefficient are very noisy and the tumors can not be separated from the other structures. The CS method was the only one to detect all lesions (from the 20 individual ones present in all studies) and all vessels present in the images. It provides a way to discriminate these two different groups of structures, assigning positive values to tumors and negative values to vessels, due to their different kinetic characteristics.

IV. DISCUSSION

In contrast to PCA, which generates different images for each structure in a dynamic study, SM depicts all these structures in one single image. The SM generation is not automatic, as in the case of PCA, since these maps represent the contrast of a lesion area versus muscle tissue, after the placement of a ROI over the lesion and the vessels respectively. The application of the COR and NCOR maps

could discriminate among structures in the dynamic phantom dataset, however they were ineffective in separating structures in clinical data. The new similarity coefficients proposed here in (6)-(9) managed to reveal all structures of interest to visual inspection. Particularly CS (9) provided better parametric images and could be the method of choice as far as the discrimination between the tumor and other structures is concerned, both on simulated phantom studies and clinical data from PET studies of colorectal tumor recurrences, even in the vicinity of hot organs such as the bladder.

Both PCA and SM methods require that the image frames for the same tomographic slice are spatially registered. In order to correctly classify voxels or volumes/regions of interest based on similarity criteria, the images should be previously checked for spatial registration. Patient motion and respiratory artifacts should be therefore corrected prior to the application of these methods on dynamic PET images.

Independent component analysis (ICA) is currently under investigation, in order to evaluate if this approach could improve further the results currently obtained. ICA is a statistical technique that can be used as a method for blind source separation. The observed data are assumed to be unknown linear mixtures of unobserved independent source signals, which can be recovered with no prior information using ICA.

ICA can be used in two complementary ways to decompose an image sequence into a set of images and a corresponding set of time-varying image amplitudes. Spatial ICA seeks a set of mutually independent component (IC) source images and a corresponding set of unconstrained time courses. Temporal ICA seeks a set of IC source time courses and a corresponding set of unconstrained images.

These conventional ICA approaches embody the assumption that the PDF of the independent sources are highly cyrtotic and symmetric. However this assumption is not warranted for dynamic PET data sets. Skew-ICA is a third approach, based on the assumption that images are characterised by the skewness (rather than the kurtosis) of their PDFs; an assumption consistent with spatially localized regions of activity.

Both PCA and ICA which are apparently data driven methods, imply a particular statistical model, whether or not this model is made explicit. The model implicit in PCA is that different modes are Gaussian and uncorrelated, whereas ICA model is that different modes are non-Gaussian and independent. Therefore, ICA is expected not only to de-correlate the signals but also reduce the higher order statistical dependencies.

V. ACKNOWLEDGEMENTS

The authors would like to thank Prof. Dr. Ludwig G. Strauss and Dr. Antonia Dimitrakopoulou-Strauss from the German

Cancer Research Center (Heidelberg, Germany) for providing the clinical data for the experiments shown in this work and for clarifying discussions.

VI. CONCLUSIONS

The PCA and SM techniques represent efficient methods for data reduction in large PET dynamic image sequences. They support visual interpretation of the dynamic studies and assist the application of compartment modeling. The methods developed represent promising alternative techniques for quantification, fast, independent of any kinetic model and useful when the retrieval of the input function is complicated. Treatment planning and assessment of angiogenesis blocking drugs using PCA and SM can be investigated. In the case of SM, manual selection of the reference ROI could be time consuming and prone to operator bias, therefore research is ongoing for the development of a semi-automatic technique for the optimum selection of reference ROI. Future work will include the investigation of the ICA methodology.

VII. REFERENCES

- [1] L. G. Strauss, and P. S. Conti, "The applications of PET in clinical oncology," *J. Nucl. Med.*, vol. 32, pp. 623-648, 1991.
- [2] J. W. Keyes, "SUV: Standard uptake or silly useless value?," *J Nucl Med*, vol. 36, pp. 1836-1839, 1995.
- [3] S-C. Huang, "Anatomy of SUV," *Nucl Med Biol*, vol. 27, pp. 643-646, 2000.
- [4] L. G. Strauss, A. Dimitrakopoulou-Strauss, and U. Haberkorn, "Shortened PET data acquisition protocol for the quantification of ^{18}F -FDG kinetics," *J. Nucl. Med.*, vol. 44, no. 12, pp. 1933-1939, 2003.
- [5] F. Pedersen, M. Bergström, E. Bengtsson, and B. Långström, "Principal component analysis of dynamic positron emission tomography images," *Eur. J. Nucl. Med.*, vol. 21, pp. 1285-1292, 1994.
- [6] J. V. Stone, J. Porril, N. R. Porter, and I. D. Wilkinson, "Spatiotemporal independent component analysis of event-related fMRI data using skewed probability density functions," *Neuroimage*, vol. 15, no. 2, pp. 407-21, Feb. 2002
- [7] J. S. Lee, D. S. Lee, J. Y. Ahn, G. J. Cheon, S-K. Kim, J. S. Yeo, et al., "Blind separation of cardiac components and extraction of input function from H_2^{15}O dynamic myocardial PET using independent component analysis," *J. Nucl. Med.*, vol. 42, no. 6, pp. 938-943, 2001.
- [8] R. A Johnson and D. W. Wichern, *Principal Components*. In: *Applied Multivariate Statistical Analysis*, New Jersey: Prentice Hall (4th ed.), pp. 458-513, 1998.
- [9] J. Rogowska, K. Jr. Preston, H. J. Aronen, and G L. Wolf, "A comparative analysis of similarity mapping and eigenimaging as applied to dynamic MR imaging of low grade astrocytoma," *Acta Radiologica*, vol. 35, pp. 371-377, 1994.
- [10] J. Rogowska, K. Preston, G. J. Hunter, L. M. Hamberg, K. K. Kwong, O. Salonen, and G. L. Wolf, "Applications of similarity mapping in dynamic MRI," *IEEE Trans. Med. Imag.*, vol. 14, pp. 480-486, 1995.